JOURNAL OF MATERIALS SCIENCE 33 (1998) 5351–5357

Friction and plasticity effects in wedge splitting and cutting fracture tests

J. G. WILLIAMS
Mechanical Engineering Department, Imperial College of Science, Technology and Medicine London, SW7 2BX, UK
E-mail: g.williams@ic.ac.uk

An analysis is given for determining G for removing a thin layer using a wedge. Corrections are described for both friction and the plastic bending of the layer. Experimental results are analysed for adhesive joints and for cutting tests on polymers and biological materials. In all of these the fracture toughness could be found. Some general observations on schemes for analysing these tests are given.

1. Introduction

There are several circumstances when a fracture is propagated by the action of a wedge or blade. There are wedge tests used to determine the fracture toughness of adhesive joints [1, 2] and, indeed, one of the earliest fracture references, by Obreimoff [3] used a wedge test to delaminate mica. A closely analogous case is that of microtomy in which thin slices are removed and the toughness determined [4–6] and also a blade scraping test for coatings [7]. The problem encountered in analysing all of them is that the work of fracture which is measured includes contributions not only from the material toughness, but also from friction and from plastic deformation, which creates curling in the removed layer. There have been some attempts to separate these effects but none have been completely satisfactory quantitatively.

The analysis described here arose from a study of the peeling of flexible laminates [8, 9] where a scheme was developed for calculating the plastic work dissipated. This same method has been used here in the wedge cutting cases together with the inclusion of friction effects.

2. Friction effects

Fig. 1a shows the general configuration of a wedge of angle α removing a layer of thickness h from a surface as a horizontal force F is applied. The effect of the wedge is to apply a vertical force P to the layer thus developing a bending moment in the layer. There are two important cases indicated in the diagram;

1. The sharp wedge ($\alpha =$ constant): In this situation α remains constant as the wedge is forced in and the contact point moves closer to the wedge tip.
2. The blunt wedge ($u =$ constant): Here the contact point is maintained at a constant height, u, above the surface and α increases as the wedge is driven in. A circular pin or radius nosed wedge are examples of this case.

These changes occur during the loading stage and during subsequent steady-state propagation both u and α remained constant with α predetermined in case 1 and in u case 2.

The angle γ shown in the diagram is a clearance angle which is used to avoid friction on the lower surface. The adhesive wedge test [1, 2] where two strips are separated is obtained by adding together two of the strips shown and having a wedge angle of 2α or a tip width of $2u$.

The forces acting on the wedge are shown in Fig. 1b and for the case of no friction on the base ($\mu P = 0$) we have,

$$F = K(\sin\alpha + \mu\cos\alpha) \quad \text{and} \quad P = K(\cos\alpha - \mu\sin\alpha)$$

i.e.,

$$\frac{F}{P} = \frac{\sin\alpha + \mu\cos\alpha}{\cos\alpha - \mu\sin\alpha} = \tan\alpha \cdot \mathrm{Z} \tag{1}$$

where

$$\mathrm{Z} = \frac{1 + (\mu/\tan\alpha)}{1 - \mu\tan\alpha}$$

If the force F moves forward a small distance $\mathrm{d}x$ then the external work input is

$$\mathrm{d}U_{\mathrm{ext}} = F \cdot \mathrm{d}x$$

For steady-state propagation the crack growth $\mathrm{d}l = \mathrm{d}x$ and for a wedge width b we have,

$$\frac{\mathrm{d}U_{\mathrm{ext}}}{b\,\mathrm{d}l} = \frac{F}{b} \tag{2}$$

The energy release rate which drives the crack is given by [8]

$$G = \frac{\mathrm{d}U_{\mathrm{ext}}}{b\,\mathrm{d}l} - \frac{\mathrm{d}U_{\mathrm{s}}}{b\,\mathrm{d}l} - \frac{\mathrm{d}U_{\mathrm{d}}}{b\,\mathrm{d}l} \tag{3}$$

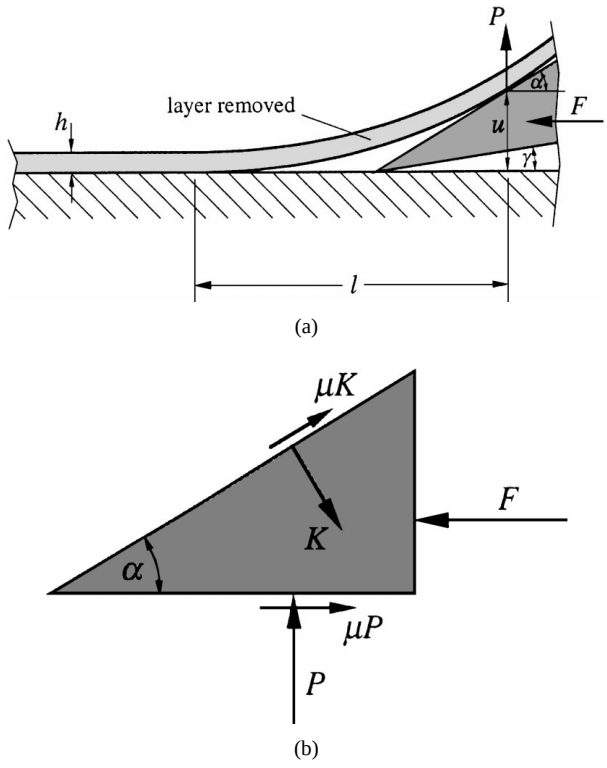

Figure 1

where U_s is the strain energy and U_d is the dissipated energy. (Dynamic effects involving kinetic energy can be included but are ignored here.)

If we assume that the layer is elastic then there are no energy changes in the layer in the steady-state, i.e., $dU_s = 0$ and $dU_d = 0$ since there is no plastic curling. However, there is energy dissipation via friction since the friction force μK moves $dx/\cos\alpha$ and hence,

$$\frac{dU_d}{b\,dl} = \frac{\mu K}{b\cos\alpha} = \frac{\mu F}{b\cos\alpha(\sin\alpha + \mu\cos\alpha)} \tag{4}$$

and hence,

$$G = \left(\frac{F}{b}\right)\tan\alpha\left(\frac{1-\mu\tan\alpha}{\tan\alpha+\mu}\right) = \left(\frac{P}{b}\right)\tan\alpha \tag{5}$$

i.e., the true energy input rate to the layer.

If it is assumed that G is constant for propagation then

$$\left(\frac{F}{b}\right) = \frac{G(\tan\alpha+\mu)}{\tan\alpha(1-\mu\tan\alpha)} = Z\cdot G.$$

For $\mu = 0$, $Z = 1$ and $F/b = G$ but for $\mu \neq 0$, $F/b \to \infty$ as $\alpha \to 0$ and also as $\alpha \to \tan^{-1}(1/\mu)$. There is a minimum value of F/b when

$$\alpha_{\min} = \tan^{-1}\left(\sqrt{1+\mu^2}-\mu\right) \tag{6}$$

and

$$\left(\frac{F}{b}\right)_{\min} = \frac{G}{\left(\sqrt{1+\mu^2}-\mu\right)^2} \tag{7}$$

For small values of μ, $\alpha_{\min} \to 45^\circ$ and decreases to only 32° at $\mu = 0.5$ with $(F/b)_{\min} = 2.6G$. It should also be noted that for $\alpha \geq \tan^{-1}(1/\mu)$ no energy release can be generated.

For the case of friction on the base, (i.e., $\mu P \neq 0$)

$$G = \frac{F}{b}\tan\alpha\left[\frac{1-\mu\tan\alpha}{(1-\mu^2)\tan\alpha+2\mu}\right] \tag{8}$$

i.e., the effect of μ is approximately doubled.

3. Elastic deformations

If the layer deforms elastically when debonded then there is no energy dissipated other than friction. For the sharp blade case with α fixed G may be found via Equation 5 by measuring F. However μ is generally unknown and one way of overcoming this problem is to make measurements of the debonded length. This was the method used by Obreimoff in 1930 [3] in which the debonded length l, see Fig. 1a, was measured. If small angles are assumed then simple beam theory may be applied since,

$$u = \frac{4Pl^3}{Ebh^3} \quad \text{and} \quad \alpha = \frac{6Pl^2}{Ebh^3}$$

The energy release rate (Equation 5) is

$$G = \frac{P}{b}\alpha = \frac{6}{Eh^3}\left(\frac{P}{b}\right)^2 l^2$$

and

$$G = \frac{Eh}{6}\left(\frac{h\alpha}{l}\right)^2 = \frac{3Eh}{8}\left(\frac{hu}{l^2}\right)^2 \tag{9}$$

Thus, if l is measured G may be found for either a fixed α or a fixed u. By measuring l one is effectively measuring the radius of curvature of the layer at the debonding point R_0 since,

$$\frac{1}{R_0} = \frac{12Pl}{Ebh^3} = \frac{2\alpha}{l} = \frac{3u}{l^2}$$

and

$$G = \frac{Eh}{24}\cdot\frac{h^2}{R_0^2} \tag{10}$$

Recent studies of peeling [8, 9] have shown that this type of local bending analysis requires a refinement in that the debonding point does not have a zero slope and displacement as assumed above. The shear force and bending moment at the base give rise to stretching and rotation of the layer, beyond the debonding point. The layer effectively acts as if it is longer than l by $\frac{2}{3}h$ so that l should be replaced by $(l+\frac{2}{3}h)$ in the above relationships and that the root slope and displacements are

$$\alpha_0 = \frac{2}{3}\frac{h}{R_0} \ll 1 \quad \text{and} \quad u_0 = \frac{2}{9}\frac{h^2}{R_0} \tag{11a}$$

giving

$$G = \frac{Eh}{24}\frac{h^2}{R_0^2}\left(1 + \frac{4}{3}\frac{h}{l}\right), \qquad \frac{1}{R_0} = \frac{2\alpha}{l\left(1 + \frac{4}{3}\frac{h}{l}\right)} \tag{11b}$$

For some cutting processes the knife angles are large (e.g., microtoming) and it is necessary to use large displacement beam analysis. The slope at any point a distance x from the debonding point on the beam is ϕ and the moment at that point is

$$M = P(l - x) + F(u - v)$$

where v is the local displacement. Noting Equation 1 and that

$$\frac{\mathrm{d}x}{\mathrm{d}\phi} = R\cos\phi \quad \text{and} \quad \frac{\mathrm{d}v}{\mathrm{d}\phi} = R\sin\phi$$

where R is the local radius of curvature [8] then

$$\frac{\mathrm{d}M}{\mathrm{d}\phi} = -PR[\cos\phi + \tan\alpha \cdot \mathrm{Z} \cdot \sin\phi]$$

From beam theory we have

$$\frac{1}{R} = \frac{12M}{Ebh^3}$$

i.e.,

$$\frac{\mathrm{d}R}{R^3} = \frac{12P}{Eh^3b}[\cos\phi + \tan\alpha \cdot \mathrm{Z} \cdot \sin\phi]d\phi$$

Integrating and noting that $R = \infty$ where $\phi = \alpha$ and $R = R_0$ at $\phi = \alpha_0$ we have

$$\frac{1}{R_0^2} = \frac{24}{Eh^3} \cdot \frac{P}{b} \cdot [(\sin\alpha - \sin\alpha_0) + \tan\alpha \cdot \mathrm{Z}(\cos\alpha_0 - \cos\alpha)]$$

where

$$\sin\alpha_0 = \frac{2}{3}\frac{h}{R_0}$$

and on substituting for G from Equation 5

$$G = \left(\frac{3}{32}Eh\right) \times \frac{\tan\alpha \sin^2\alpha_0}{[(\sin\alpha - \sin\alpha_0) + \tan\alpha \cdot \mathrm{Z}(\cos\alpha_0 - \cos\alpha)]} \tag{12}$$

i.e., a more precise version of Equation 10 though now μ does have an effect via Z.

It should also be noted that for small angles the sharp blade case is

$$\frac{F}{b} \approx G\left(1 + \frac{\mu}{\alpha}\right)$$

i.e., independent of h for a constant G. For blunt blades

$$\alpha = 3\left(\frac{u}{h}\right)^{1/2}\left(\frac{G}{6Eh}\right)^{1/4}$$

and hence F/b will be proportional to $h^{3/4}$ for $\mu \neq 0$ on substituting for α.

In all these elastic cases, observation would show that there would be no residual radius of curling in the debonded layer. If there is curling present then plastic deformation is present.

4. Plasticity effects

Plastic energy dissipation will occur in the debonded layer when the bending strain exceeds the yield strain ε_y. The onset occurs when

$$\frac{1}{R_0} = \frac{2\varepsilon_y}{h}$$

which, from Equation 10 is when

$$G = \frac{E\varepsilon_y^2 h}{6} = \frac{\sigma_y \varepsilon_y h}{6}$$

where $\sigma_y = E\varepsilon_y$ the yield stress. We shall limit our attention here to the case when there is a large amount of permanent curvature induced and assume that the radius of curvature remains at R_0 as shown in Fig. 2. There will be a small increase in R_0 due to elastic unloading, but this will be ignored. If we now assume power law work hardening of the form,

$$\sigma = \sigma_0 \varepsilon^n$$

then the plastic moment M_p may be calculated for a linear strain distribution as shown in Fig. 3, i.e.,

$$M_p = b\int_{-\frac{h}{2}}^{+\frac{h}{2}} \sigma_0\left(\frac{y}{R_0}\right)^n \cdot y \cdot \mathrm{d}y = \frac{b\sigma_0 h^2}{4}\left(\frac{2}{2+n}\right)\left(\frac{h}{2R_0}\right)^n \tag{13}$$

The plastic work done per unit length of layer is thus,

$$\frac{\mathrm{d}U_p}{\mathrm{d}a} = \int_0^{\frac{1}{R_0}} M_p\,\mathrm{d}\left(\frac{1}{R_0}\right) = \frac{b\sigma_0 h^2}{4R_0}\frac{2}{(2+n)(1+n)}\left(\frac{h}{2R_0}\right)^n \tag{14}$$

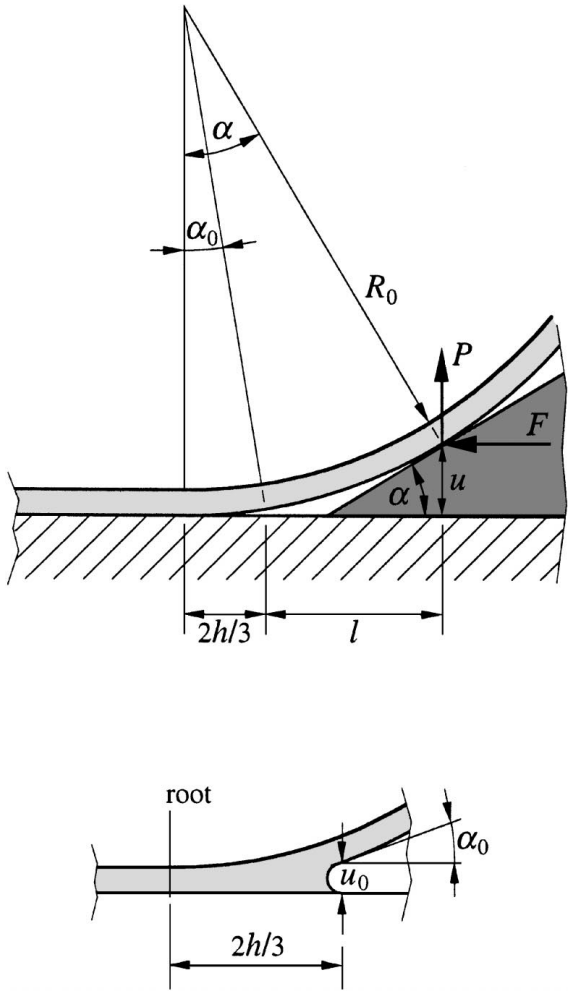

Figure 2

i.e.,

$$\frac{\mathrm{d}U_p}{b\,\mathrm{d}a} = \bar{G}(\sin\alpha_0)^{1+n},$$

$$\bar{G} = \left(\frac{3}{4}\right)^{1+n} \frac{\sigma_0 h}{(2+n)(1+n)}$$

This plastic work is also dissipated so the true G in Equation 5 now becomes

$$G = \frac{P}{b} \cdot \tan\alpha - \frac{1}{b}\frac{\mathrm{d}U_p}{\mathrm{d}a} \tag{15}$$

For large displacements from Fig. 3 we have

$$l = R_0(\sin\alpha - \sin\alpha_0) \quad \text{and} \quad u = R_0(1 - \cos\alpha)$$

and

$$M_p = Pl + F(u - u_0)$$

Thus

$$\frac{M_p}{bR_0} = \frac{P}{b}[(\sin\alpha - \sin\alpha_0) + \tan\alpha \mathrm{Z}(\cos\alpha_0 - \cos\alpha)]$$

$$= (1+n)\frac{1}{b}\frac{\mathrm{d}U_p}{\mathrm{d}a} \tag{16}$$

and on substituting in Equation 15;

$$G = \bar{G}(\sin\alpha_0)^{1+n} \times \left[\frac{(1+n)\tan\alpha}{[(\sin\alpha - \sin\alpha_0) + \tan\alpha \mathrm{Z}(\cos\alpha_0 - \cos\alpha)]} - 1\right] \tag{17}$$

If R_0 or l and h are measured directly then α_0 and hence G may be found since

$$\sin\alpha_0 = \frac{2}{3}\frac{h}{R_0} = \left(\frac{2}{3}\frac{h}{l} \Big/ 1 + \frac{2}{3}\frac{h}{l}\right)\sin\alpha$$

For blunt wedges and small angles this becomes

$$G = \frac{\sigma_0 h}{(2+n)(1+n)}\left(\frac{h}{2R_0}\right)^{1+n} \times \left[n + \frac{2}{3}\frac{h}{\sqrt{2uR_0}} \Big/ 1 - \frac{2}{3}\frac{h}{\sqrt{2uR_0}}\right] \tag{18}$$

and by measuring R_0 directly G may be found.

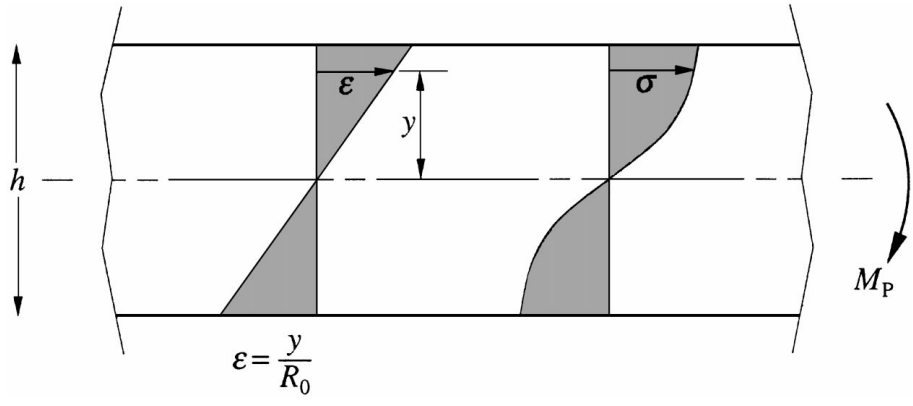

Figure 3

If F is measured we have,

$$\frac{F}{b} = \mathrm{Z}[G + \bar{G}(\sin\alpha_0)^{1+n}] \tag{19}$$

and $(\sin\alpha_0)$ may be determined from Equation 17.

Two special cases for the sharp wedge are of interest. For low dissipation, i.e., $\bar{G} \ll G$ and/or high friction, i.e., $\mathrm{Z} \gg 1$, $\alpha_0 \to \alpha$ and Equation 19 then becomes,

$$\frac{F}{b} = \mathrm{Z}[G + \bar{G}(\sin\alpha)^{1+n}] \tag{20}$$

and F/b will have a linear dependence on h from $\bar{G}$. For large dissipation i.e., $\bar{G} \gg G$ and/or lower Z, $\sin\alpha_0$ is small and for $n \to 0$ Equation 17 gives,

$$(\sin\alpha_0)^2 \to \frac{G}{G}\tan\alpha[\mathrm{Z} - (\mathrm{Z}-1)\cos\alpha]$$

and

$$\frac{F}{b} = Z\left[G + \sqrt{G \cdot \bar{G} \cdot \tan\alpha[\mathrm{Z} - (\mathrm{Z}-1)\cos\alpha]}\right] \tag{21}$$

i.e., F/b is proportional to $\sqrt{h}$ from $\bar{G}$. For $n \neq 0$ the dependence becomes $h^{1/(2+n)}$.

The transition from linear to square root thickness dependence will be approximately, when

$$h = \bar{h} = \left(\frac{8G}{3\sigma_0}\right)\frac{[\mathrm{Z} - (\mathrm{Z}-1)\cos\alpha]}{\sin\alpha \cdot \cos\alpha} \tag{22}$$

For the small angle α, blunt wedge, case the solution becomes,

$$\frac{F}{b} = G^{1/3} \times \left[G^{1/3} + \frac{\mu}{\sqrt{3}}\frac{h}{u}\left(\frac{3}{8}\sigma_0 u\right)^{1/3}\right]\left[G^{1/3} + \left(\frac{3}{8}\sigma_0 u\right)^{1/3}\right] \tag{23}$$

5. Comparisons with experiments

The first set of data to be considered is that of Thouless *et al.* [2] in which metal strips were wedged apart as shown in Fig. 4 and the radii of curvature R_0 were measured for various thicknesses of strip h. Two metals, a steel and an aluminium alloy were used and three adhesives, coded A, B and C. Power law work hardening was used to describe the properties so the appropriate relationship is Equation 18 with a factor of two for the two arms, which can be rearranged as,

$$G = \left[\frac{\sigma_0}{1+n}\left(\frac{h}{2R_0}\right)^n\right]\left(\frac{h^2}{R_0}\right)\frac{1}{2+n} \times \left[n + \frac{2}{3\sqrt{2u}}\left(\frac{h^2}{R_0}\right)^{1/2} \Big/ 1 - \frac{2}{3\sqrt{2u}}\left(\frac{h^2}{R_0}\right)^{1/2}\right] \tag{24}$$

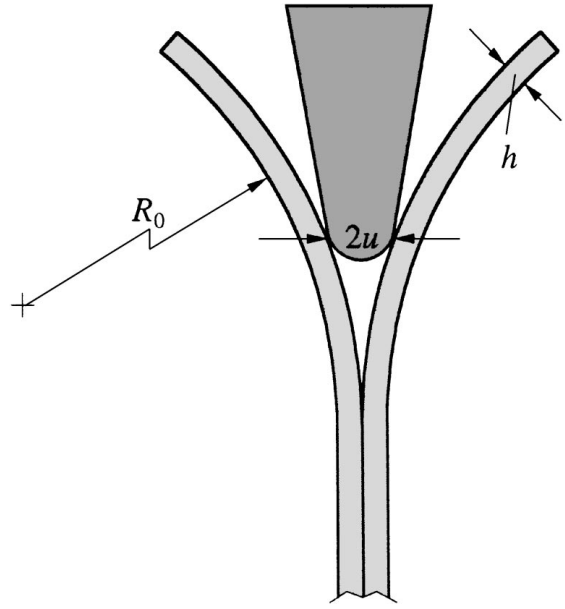

Figure 4

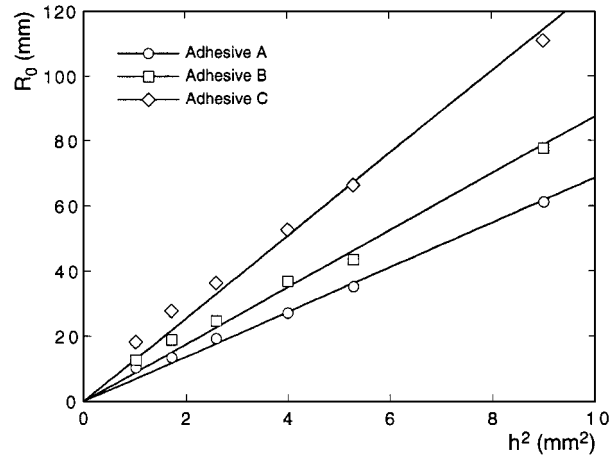

(a)

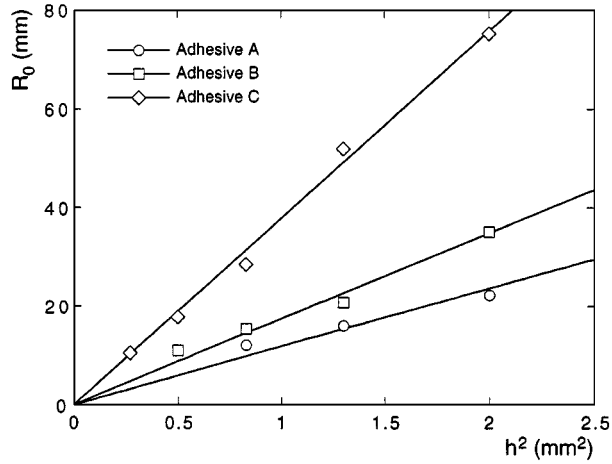

(b)

Figure 5

The parameter $\bar{\sigma} = h\int_{-(h/2)}^{+(h/2)} \sigma\,\mathrm{d}y = (\sigma_0/1+n)(h/2R_0)^n$ is the mean stress in the layer and varies only slightly so that for a constant G, h^2/R_0 will be constant and Fig. 5a and b show R_0 versus h^2 where good linearity is observed.

TABLE I

Adhesive	h^2/R_0 (mm)	$\bar{\sigma}$ (MPa)	G (kJ/m^2)
	Aluminium alloy $u = 1$ mm, $\sigma = 377\ \varepsilon^{0.25}$ MPa		
A	0.148	133	4.6
B	0.116	125	3.2
C	0.079	114	1.8
	Steel $\sigma = 426\ \varepsilon^{0.13}$ MPa		
A	0.083	243	2.9
B	0.055	235	1.6
C	0.026	219	0.6

The slopes h^2/R_0 are given in Table I together with average values of $\bar{\sigma}$ for each case. These latter are not constant but vary by only $\pm 10\%$. The values of the computed values of G are also given. It is of interest that the values of G are clearly different for the different substrates. Values of G for adhesives A and B on aluminium have been reported [10] as 4.1 kJ/m^2 and 2.5 kJ/m^2, respectively.

Instrumented microtome machines have been proposed as methods for determining the fracture toughness of soft materials [4, 5]. In most cases thin layers of varying thickness are removed and (F/b) is recorded. The blades are very sharp with tip radii as small as 10 nm and the blade tip angles are about 40° to provide the necessary blade stiffness. It is necessary also to give some clearance (γ in Fig. 1) so the total blade angle α in about 50° in most cases necessitating the use of the large angle solution. A good set of data, taken from [5], is shown in Fig. 6 and shows F/b as a function of h for wood and liver.

In both cases straight lines were drawn and the intercepts taken as G [5]. Such linearity is the case modelled by Equation 20 which may be written as,

$$\frac{F}{b} = \mathrm{Z}G + \mathrm{Z}\frac{3}{8}\sin\alpha \cdot \sigma_0 \cdot h$$

for $n = 0$.

For the blades used $\alpha \approx 54°$ and the slope is thus about $0.3\ \sigma_0$. For the wood data this slope is 6.1 MPa. It is not easy to define a yield stress for wood but it can generally be taken as at least 50 MPa. Since $\mathrm{Z} \geq 1$ it can be seen that the linear fit is not reasonable. Indeed curvature is apparent in the data and a more sensible form is Equation 21 which is,

$$\frac{F}{b} = \mathrm{Z}G + \mathrm{Z}\sqrt{\tan\alpha[\mathrm{Z} - (\mathrm{Z}-1)\cos\alpha]G\frac{3}{8}\sigma_0}\sqrt{h}.$$

This line is shown fitted in Fig. 6 with,

$$\mathrm{Z}G = 28\ \mathrm{J/m^2}$$

and

$$\mathrm{Z}\sqrt{\tan\alpha[\mathrm{Z} - (\mathrm{Z}-1)\cos\alpha]G\frac{3}{8}\sigma_0} = 43 \times 10^3\ \mathrm{J/m^2\ m^{1/2}}$$

Assuming $\sigma_0 \approx 50$ MPa we have $\mathrm{Z} = 1.9$ and since,

$$\mathrm{Z} = 1 + (\mu/\tan\alpha)/1 - \mu\tan\alpha,$$

$\mu = 0.26$ and finally $G = 15$ J/m^2. The transition to linear behaviour is given by Equation 22;

$$\bar{h} = \frac{G}{\sigma_0}\left[\frac{8}{3}\frac{[\mathrm{Z} - (\mathrm{Z}-1)\cos\alpha]}{\sin\alpha \cdot \cos\alpha}\right]$$

and hence becomes 2.3 μm. The linear region with $\bar{h}$ is also shown in Fig. 6.

The liver data is more difficult to analyse, since no yield stress data is known but certainly σ_0 is very small and no greater than 1 MPa. There is no detectable curvature in the data but the range of h is small. The slope gives,

$$\mathrm{Z}\sigma_0 = 18\ \mathrm{MPa}$$

which suggests a very high Z, and hence high μ values, giving the observed linearity and very low G values, i.e., < 2 J/m^2, which are sensible.

Fig. 7 shows data for various polymers, taken from [6] where an ultramicrotome was used giving slices in the range 0.05–0.2 μm. The yield stresses are not given, but for the materials used they are all about 100 MPa. At small thicknesses there is reasonable linearity and the slopes and intercepts are given in Table II.

Also shown are the values of Z, μ and G deduced assuming $\sigma_0 = 100$ MPa. The values of G are very small and, as discussed in [6], probably represent true fracture energies for these materials, because plastic energy dissipation cannot occur in these very thin layers.

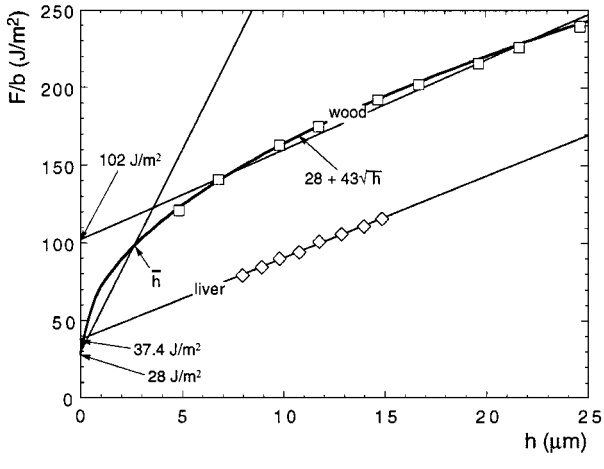

Figure 6

TABLE II Polymer ultramicrotome data from [6]

	$\sigma_0 = 100$ MPa				
Material	Intercept (J/m^2)	Slope (MPa)	Z	μ	G (J/m^2)
Epoxy A	22	377	12.6	0.63	1.7
Epoxy B	20	140	4.7	0.51	4.2
PMMA	18	207	6.9	0.57	2.7
PS	13	83	2.8	0.39	4.7

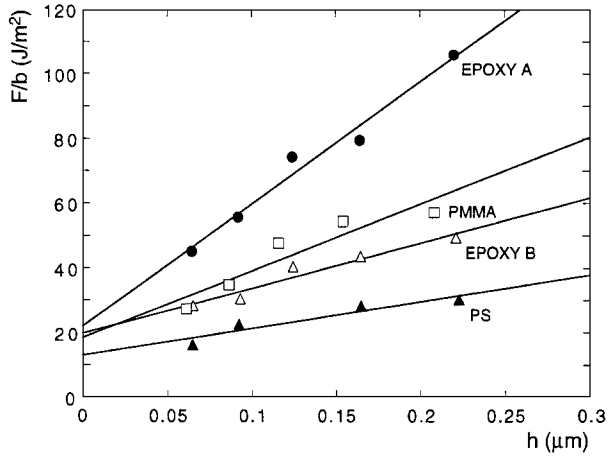

Figure 7

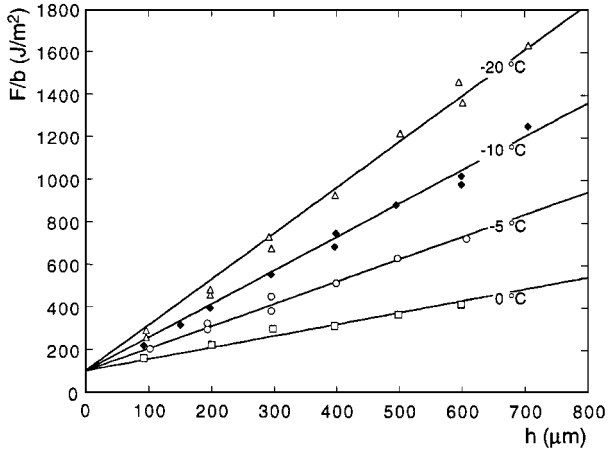

Figure 8

TABLE III Frozen meat data from [11]

Temp (°C)	Intercept (J/m^2)	Slope (MPa)	σ_0 (MPa)	Z	μ	G (J/m^2)
−20	100	2.1	4.5	1.6	0.20	62
−10	100	1.6	1.4	3.8	0.46	26
−5	100	1.0	0.6	5.6	0.54	18
0	100	0.5	0.2*	8.3	0.59	12

*Extrapolated.

As a final example Fig. 8 shows data from [11] taken on frozen meat at four temperatures. The thicknesses are quite large because of the inhomogeneous nature of the material, but good linearity is observed. The slopes and intercepts are given in Table III together with σ_0 values which are given in [11].

Z and hence μ values are shown which are deduced from the slopes and σ_0 indicating a reduction in friction at low temperatures where the meat is more rigid. G shows an increase with decreasing temperature presumably because of the ice formed. The high friction implied in the liver data is supported by these results.

6. Conclusions

The analysis and results given here suggest that it is possible to determine G via wedge or cutting tests. However in order to make the necessary corrections the stress-strain properties must be known. A simple extrapolation of force per unit width to zero thickness is fraught with dangers in terms of identifying linearity and correcting the intercept. If both the yield stress and the friction are unknown then it is not possible to have any confidence in the results. When σ_0 is known it does appear possible to deduce μ and hence make corrections for both linear and square root thickness dependence. The more direct method of measuring the radius of curvature, either under load or subsequently, has many attractions since it is much less sensitive to friction than schemes using force. One may also measure both P and F directly in order to define Z and hence the friction contribution. The most successful methodology would appear to be to measure forces as a function of thickness, determine the stress-strain curve and also measure the curvature. Such schemes would provide sufficient cross checks to give confidence in the values obtained.

References

1. A. J. TAYLOR, B. R. K. BLACKMAN, A. J. KINLOCH and Y. WANG, in Conf. Proc. of Structural Adhesives in Engineering IV (Institute of Materials, London, 1995).
2. M. D. THOULESS, J. L. ADAMS, M. S. KAFKALIDIS, M. WARD, R. A. DICKIE and G. L. WESTERBEEK, *J. Mater. Sci.* **33** (1998) 189–197.
3. J. W. OBREIMOFF, *Proc. Roy. Soc.* **A127** (1930) 290–297.
4. A. G. ATKINS and J. F. V. VINCENT, *J. Mater. Sci. Lett.* **3** (1984) 310–312.
5. A. WILLIS and J. F. V. VINCENT, *J. Microscopy* **178** (1995) 56–65.
6. M. L. ERICSON and H. LINDBERG, *J. Mater. Sci.* **31** (1996) 655–662.
7. W. K. ASBECK, *Paint and Varnish Production* (March 1970) 23–29.
8. J. G. WILLIAMS, *J. Adhesion* **41** (1995) 225–239.
9. A. J. KINLOCH, C. C. LAU and J. G. WILLIAMS, *Int. J. Fracture* **66** (1994) 45–70.
10. A. J. KINLOCH, B. R. K. BLACKMAN, A. J. TAYLOR and Y. WANG, in Conf. Proc. of 'Adhesion '96' (Institute of Materials, London, 1996) p. 467.
11. B. J. DOBRASZCZYK, A. G. ATKINS, G. JERONIMIDIS, and P. P. PURSLOW, *J. Mater. Sc.* **21** (1987) 25–49.

Received 11 September
and accepted 11 September 1998